

## Heterogeneous Polypropylene-Based Cation-Exchange Membrane Modified by Functionalized Zinc Oxide Particles for Vanadium Redox Flow Battery

Khoiruddin Khoiruddin<sup>1), 2), \*</sup>, Rizky Wahyu Firmansyah<sup>1)</sup>, Nanda Yulanda<sup>1)</sup>,  
Anita Kusuma Wardani<sup>1)</sup>, I Gede Wenten<sup>1), 2)</sup>

<sup>1)</sup>Chemical Engineering Department, Institut Teknologi Bandung, Jalan Ganesa No. 10, Bandung 40132, Indonesia

<sup>2)</sup>Research Center for Nanosciences and Nanotechnology, Institut Teknologi Bandung, Jalan Ganesa No. 10, Bandung 40132, Indonesia

<sup>\*</sup> Corresponding author: khoiruddin@itb.ac.id

(Received: 09 October 2024; Accepted: 17 February 2025; Published: 28 February 2025)

### Abstract

*This work presents the synthesis and characterization of heterogeneous cation-exchange membranes based on polypropylene (PP) and cation-exchange resin (IER) powder, developed via melt spinning technique. The membranes were modified with zinc oxide (ZnO) nanoparticles functionalized with polydopamine (PDA) for their electrochemical properties enhancement. The effects of IER content and ZnO/PDA loading variations on the key membrane properties, including ion-exchange capacity (IEC), water uptake (WU), water contact angle (WCA), proton conductivity, water permeability, and vanadium permeability, were investigated. The results demonstrated that increase in IER content improved proton conductivity, IEC, and vanadium permeability. The PP/ZnO-PDA membrane, with 2.5 wt.% ZnO/PDA (Z-2.5), showed reduced water permeability ( $<0.5 \text{ L}\cdot\text{m}^{-2}\cdot\text{h}^{-1}\cdot\text{bar}^{-1}$ ) and vanadium permeability ( $<6 \times 10^{-5} \text{ cm}^2 \text{ min}^{-1}$ ), while maintaining moderate proton conductivity ( $\sim 13 \text{ mS/cm}$ ). Nevertheless, the increase in ZnO/PDA content beyond 2.5 wt.% led to the reduction of WU, IEC, and proton conductivity, which is likely due to the aggregation of nanoparticle and subsequently reduces the access to ion-exchange sites.*

**Keywords:** energy storage; functionalized nanomaterial; ion transport; polymer

**How to Cite This Article:** Khoiruddin, K., Firmansyah, R.W., Yulanda, N., Wardani A. K., Wenten, I G. (2024), Heterogeneous Polypropylene-Based Cation-Exchange Membrane Modified by Functionalized Zinc Oxide Particles for Vanadium Redox Flow Battery, Reaktor, 24 (2), 58 - 67, <https://doi.org/10.14710/reaktor.24.2.58-67>

### INTRODUCTION

Currently, numerous renewable energy sources have been explored as alternatives to fossil fuels (Wenten et al., 2024). However, the available renewable energy sources are generally intermittent, necessitating energy storage systems to balance between the demand and supply. The vanadium redox

flow battery (VRFB) is a membrane-based energy storage technology recognized for its high energy efficiency, large capacity, and long cycle life (Wang et al., 2024). The critical component of the VRFB is the ion-exchange membrane, which serves as a selective barrier allowing protons to pass while preventing vanadium ion crossover between the anode and

cathode compartments. This property is essential for maintaining battery efficiency and longevity, as vanadium ion crossover can lead to capacity loss and reduced performance (Jiang & Xue, 2023). To fulfill its role effectively, the membrane must exhibit high proton conductivity, low vanadium permeability, excellent chemical and mechanical stability, and cost-effectiveness (Li et al., 2023). Despite these requirements, ion-exchange membranes commonly used in VRFBs still face challenges, including high water and electrolyte ion permeability, which hinder their long-term performance stability (Oreiro et al., 2025).

Various efforts have been made to overcome these problems, including finding alternative materials, modifying of the membrane surface, and incorporating nanoparticles to the membrane matrix. Among those options, incorporation of nanoparticles into membrane matrix with additive blending is relatively simple and low-cost method for modifying membrane properties. For example, a functionalized nano-porous metal-organic framework (MOF) has been used to modify Nafion membranes through additive blending techniques (Choi et al., 2022). The result shows that the presence of the functionalized MOF was confirmed to be able to reduce the vanadium crossover of the Nafion membrane. Nafion membrane with a suppressed vanadium crossover was also reported by Cui et al. (Cui et al., 2022) who introduced tertiary amine-modified graphene oxide in the Nafion membrane matrix. The existence of fillers with positive charges may be the possible factor that restricts vanadium permeation through the membrane. Other successful works can be found elsewhere (Liang et al., 2022; Palanisamy & Oh, 2022; Zhai et al., 2022).

Ion-exchange membranes are typically available in both homogeneous and heterogeneous types. While heterogeneous membranes generally exhibit lower electrochemical properties, such as conductivity and perm-selectivity, they are easier to fabricate and more cost-effective (Khoiruddin et al., 2020). Heterogeneous membranes are fabricated by blending charged polymers, such as ion-exchange resin powder, with non-charged polymers that provide the structural framework for the membrane. In this study, commercially available cation-exchange resin, Amberlite IR 120 Na, was chosen as the ion-exchange resin. Powder cation-exchange resin provides the necessary functional charges to the membrane, which can be adjusted by altering the composition. Additionally, the presence of functional charges plays a key role in regulating ion transport in VRFB (Yang et al., 2024).

Polypropylene is one of polymeric materials that have been widely used in membrane preparation. It has excellent chemical and mechanical properties with lower fabrication cost. In this work, heterogenous cation-exchange membrane is synthesized from polypropylene and ion-exchange resin powder via melt spinning technique. The resin loading is varied

and the effect of resin loading on membrane properties is investigated. Polypropylene has high mechanical and thermal stability, with excellent chemical resistance. However, it is highly hydrophobic, which results in low conductivity in the synthesized membrane. Therefore, the membrane is also modified by incorporating polydopamine (PDA) functionalized ZnO. Zinc oxide has been widely used to modify ion-exchange membrane. It has high conductivity and high hydrophilicity (Li et al., 2024; Yan et al., 2024). Here, zinc oxide particles are coated by polydopamine, to improve the functionality of ZnO in the membrane matrix. Like ZnO, PDA is also highly hydrophilic (Alkhouzaam et al., 2021; Kugarajah et al., 2021; Wardani et al., 2019a, Wardani et al., 2020a; Yang et al., 2022). Moreover, PDA is easy to coat onto various surfaces and materials and is simple to fabricate. By combining ZnO/PDA, the synthesized heterogeneous ion-exchange membrane is expected to exhibit enhanced electrochemical properties. Furthermore, the positive charge on PDA may restrict vanadium ion permeation through the membrane, thereby reducing vanadium crossover.

## MATERIALS AND METHODS

### Materials

Granular polypropylene (from local supplier) and cation-exchange resins (Amberlite IR 120 Na) were used for heterogeneous cation-exchange membrane fabrication. ZnO (from local supplier) having average size of 300 nm was used as additive. Dopamine-HCl (Sigma-Aldrich,  $\geq 98.0\%$ ), buffer Trizma-HCl pH 8.5 (Sigma-Aldrich,  $\geq 99.0\%$ ), and isopropyl alcohol (IPA) were used for ZnO coating. Vanadyl sulphate (Shanghai Huating Chem., China), magnesium sulphate (Emsure, Merck KGaA, Darmstadt, Germany), hydrochloric sulphate (Emsure, Merck KGaA, Darmstadt, Germany), NaCl (Emsure from Merck KGaA, Darmstadt, Germany), NaOH (Emsure, Merck KGaA, Darmstadt, Germany), HCl (Pro analysis from Merck KGaA) and demineralized water were used for membrane characterization.

### ZnO/PDA Preparation

PDA solution was synthesized as per procedures reported in (Wardani et al., 2019b, Wardani et al., 2020b). About 3 g of Dopamine-HCl and in 1000 mL Trizma-HCl 20 mM, pH 8.5 were mixed until homogeneous. ZnO particles were soaked in IPA for 10 min followed by immersing in the solution for 3 h. Then, the solution was agitated at 500 rpm. Afterward, coated ZnO was washed by IPA and demineralized water for 10 min and 30 min, respectively, to remove the remaining uncoated PDA.

### Heterogenous Cation-Exchange Membrane Fabrication

Firstly, granular polypropylene (PP), cation-exchange resin powder, and ZnO/PDA particles were blended in an extruder. The ZnO/PDA was introduced

during this step to ensure uniform dispersion throughout the membrane matrix. The temperature of the extruder was set at 170°C. Then, the mixture is formed into cylindrical pellets with a diameter of 3 mm and a length of 5 mm. Here, the pellets produced from the first step had a low level of homogeneity. The pellets were fed back into the extruder and reshaped. This process was repeated three times to ensure homogeneous mixture. After obtaining homogeneous mixture, the pellet was molded into a thin sheet with the same temperature condition. Membrane compositions are summarized in Table 1.

Table 1. Membrane compositions

Membrane code	IER/PP ratio (wt.%)	ZnO-PDA content (ZnO-PDA: total solids; wt.%)
R-50	50:50	0
R-55	55:45	0
R-60	60:40	0
R-65	65:35	0
Z-2.5	50:50	2.5
Z-5	50:50	5.0
Z-7.5	50:50	7.5
Z-10	50:50	10.0

### Membrane Characterization

Membrane characterization includes water uptake (WU), water contact angle (WCA), ion-exchange capacity (IEC), proton conductivity, water permeability, vanadium ( $\text{VO}^{2+}$ ) permeability, Scanning Electron Microscope (SEM), Energy Dispersive X-Ray Spectroscopy (EDS) and Fourier-transform Infrared Spectroscopy (FTIR) analysis.

The membrane thickness was measured by a dial thickness gauge (Syntek; precision 0.01 mm). The results of the measurement show that the membranes thickness ranged between 0.5 to 1.0 mm.

To determine IEC, the membrane was firstly equilibrated in a 0.5 M HCl solution overnight to convert it from the salt form to the  $\text{H}^+$  form. Then, the membrane was immersed in a 1 M NaCl solution for 24 h. The membrane was then rinsed with demineralized water. The total volume of the rinsed water and NaCl solution were measured. A carefully taken 5 mL of the solution was titrated with HCl solution and phenolphthalein was used as the indicator. Then, the volume of the HCl solution required for the titration was recorded. The IEC was calculated based on the volume and concentration of HCl required during the titration, the total volume of NaCl solution used to immerse the membrane and volume of rinse water, and the dry weight of the membrane.

WU was determined by measuring the difference between the wet and dry weights of the membrane. The membrane was first dried in an oven at 60°C for approximately 24 hours to ensure complete removal of moisture. After drying, the membrane was

weighed to record its dry weight ( $W_{\text{dry}}$ ). Subsequently, the dried membrane was immersed in demineralized water for 24 hours at room temperature (approximately 25°C) to achieve full hydration. After immersion is completed, the membrane was gently blotted with filter paper to remove excess surface water and then weighed to obtain its wet weight ( $W_{\text{wet}}$ ).

The fixed ion concentration (FIC) represents the density of fixed ionic groups within the hydrated membrane and is an important parameter for evaluating membrane performance. FIC was calculated by dividing IEC by WU ( $\text{FIC} = \text{IEC}/\text{WU}$ ).

The WCA was determined by using procedure reported in (Jansen, 2016). A droplet of demineralized water (5  $\mu\text{L}$ ) was placed onto the membrane with a micro-syringe (Hamilton 80600 710N). The water droplet image was then captured with a digital USB microscope. The water angle is then measured by using an ImageJ processing software (Wayne Rasband). The water contact angle was measured three times on the different part of the membrane surface and on two membrane samples.

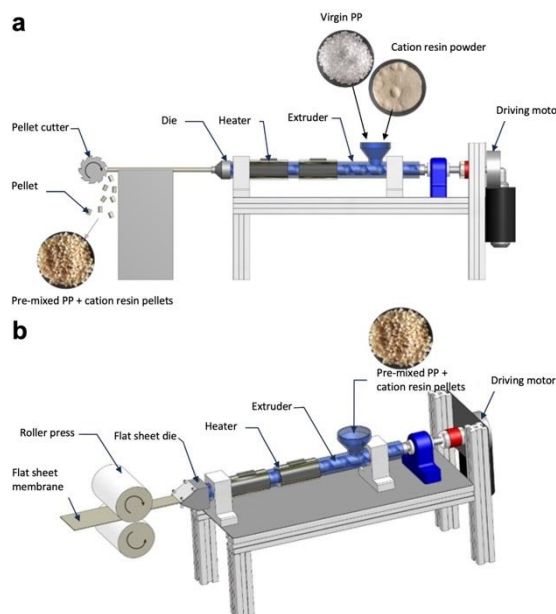


Figure 1. Set-up for membrane fabrication. (a) pelletizer (b) membrane moulding.

Water permeability of the membrane was characterized by filtration method. The membrane was placed in a dead-end filtration module and pressurized. Every 15 minutes, permeate was collected and weighed. The volume of the collected water permeate was collected in a specific time and the membrane water flux ( $J_w$ ) was calculated by equation:

$$J_w = \frac{V_p}{A \times t} \quad (1)$$

where  $V_p$  is permeate volume (L),  $A$  is membrane area ( $m^2$ ), and  $t$  is filtration time. Then, water permeability was determined by the slope of  $J_w$  vs transmembrane pressure,  $\Delta P$  (bar).

Membrane conductivity was measured according to reference (Long et al., 2020). The membranes were immersed in 1.0 M HCl for 24 h. Then, the membrane cell or module was filled with 20 mL of 0.5 M  $H_2SO_4$ . Finally, the impedance values of the conductivity cells with and without the membrane was measured by using electrochemical impedance spectroscopy (EIS, *Gamry Instrument*). The EIS measurements were conducted under the following conditions: frequency of 1-105 Hz, an electrode area of 1.8  $cm^2$ , an applied voltage of 10 mV (RMS), and a current of 1 mA (RMS). The area resistance ( $AR$ ,  $\Omega cm^2$ ) and proton conductivity were calculated according to formulas (2) – (3):

$$AR = (R_1 - R_0)A' \quad (2)$$

$$\sigma = \frac{d}{AR} \quad (3)$$

where  $A'$  is the effective area (1.8  $cm^2$ ) of membrane,  $R_1$  and  $R_0$  represent the impedance vales of the conductivity cells with and without the membrane, respectively.

The vanadium permeability was measured according to (Ye et al., 2021). The two permeation cells were separated by a membrane. The left and right permeation cells were filled with 40 mL of 1.5 M  $VO^{2+}$  + 3.0 M  $H_2SO_4$  solution and 40 mL of 1.5 M  $MgSO_4$  + 3.0 M  $H_2SO_4$  solution, respectively. Then the absorbance of the right permeation cell solution was measured by using UV-vis spectrophotometer (Genesys 10, Thermo Electron Corporation, USA) at 576 nm every 30 min. The vanadium permeability was calculated according to equation (4).

$$V \frac{dC_t}{dt} = A \frac{P}{d} (C_0 - C_t) \quad (4)$$

where  $V$  is the solution volume (40 mL) in every permeation cell, and  $A$  indicates the effective area (2.0  $cm^2$ ) of membrane.  $C_0$  is the initial concentration (1.5 mol  $L^{-1}$ ) of  $VO^{2+}$  in the left permeation cell, and  $C_t$  represents the concentration of  $VO^{2+}$  at time  $t$  (min) in the right permeation cell.  $d$  (cm) indicates the thickness of membrane.

The morphology of the membrane cross-section was probed by scanning electron microscopy (JEOL JSM 6510 LA) while the chemical properties was analysed by energy-dispersive X-ray spectroscopy (JEOLJSM 6510 LA) and Fourier transform infrared analysis (The PerkinElmer SpectrumTwo).

## RESULTS AND DISCUSSION

### Morphology and Chemical Structure of PP-based Heterogeneous Cation-Exchange Membranes

The morphology and chemical structure of the membranes were analyzed using SEM, EDS, and FTIR, as illustrated in Figures 2 and 3. SEM images reveal significant differences in the structural features of R-50 and Z-10 membranes. The R-50 membrane, with a thickness of approximately 450  $\mu m$ , displays large embedded particles (100–200  $\mu m$ ) attributed to Amberlite IR 120 Na cation resin. In contrast, the Z-10 membrane exhibits a slightly increased thickness of 500  $\mu m$ , reflecting the influence of ZnO incorporation. The observed color change from light brown in the R-50/Z-0 membrane to dark brown/black in the Z-10 membrane further supports the successful inclusion of ZnO-PDA nanoparticles.

EDS analysis (Figure 3a and 3b) provides quantitative evidence of the elemental composition of the membranes. For the R-50/Z-0 membrane, the predominant carbon peak corresponds to the polypropylene matrix. The Z-10 membrane shows additional peaks for nitrogen, oxygen, and zinc, confirming the integration of ZnO-PDA. However, the detected zinc content (0.12 wt.%) is lower than expected, likely due to the limitations of EDS in quantifying elements within thick membranes (~0.5 mm) (Mohammed & Abdullah, 2018). Furthermore, ZnO nanoparticles may have aggregated during synthesis, leading to non-uniform distribution, as noted in similar studies (Mezher et al., 2024).

FTIR spectra (Figure 3c) reveal key chemical features of the membranes. Strong peaks at 2910  $cm^{-1}$ , 1453  $cm^{-1}$ , and 1375  $cm^{-1}$  confirm the presence of C-H bonds and aliphatic chains, characteristic of polypropylene. Additional peaks at 1644  $cm^{-1}$  and 1534  $cm^{-1}$ , attributed to N-H bending and C=C bonds, respectively, indicate the incorporation of PDA and ZnO (Liu et al., 2016). These features confirm the successful modification of the PP matrix with ZnO-PDA, enhancing the membrane functional properties.

The absence of sulfur peaks in the EDS spectra, despite the presence of  $SO_3$  groups in Amberlite resin, highlights the limitations of EDS in detecting light elements in low concentrations. This discrepancy could also result from the non-uniform distribution of sulfur within the membrane, reflecting challenges in achieving homogeneous dispersion of ion-exchange resin particles.

### Effects of Ion-Exchange Resins Content

The effect of variation of ion-exchange resin concentrations on membrane properties is presented in Figure 4. An increase in resin content (R-50 to R-65) significantly enhances water uptake, IEC, and conductivity. This correlation arises from the introduction of more functional groups associated with the ion-exchange resin, as previously documented (Vyas et al., 2003). Water uptake increases due to the hydrophilic nature of the resin, promoting water retention within the membrane matrix. IEC values follow a similar trend, reflecting the higher availability of ion-exchange sites.

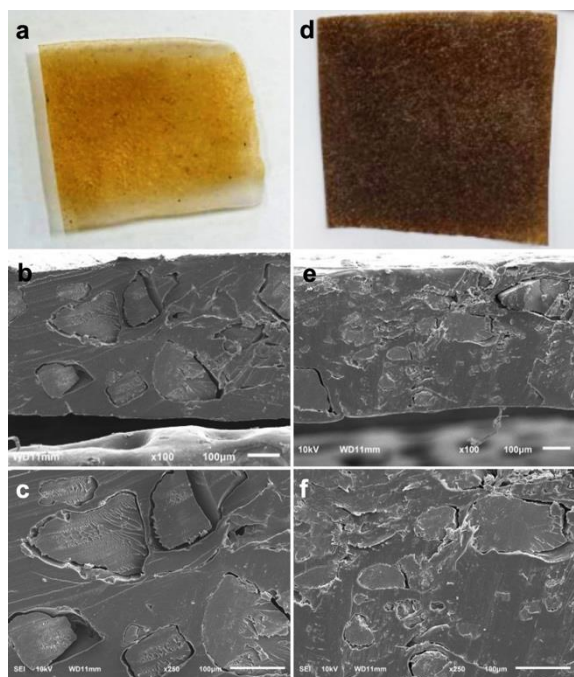


Figure 2. (a, b) Photographs and (c-f) SEM images of membrane cross-section. (a, b, c: PP membrane; d, e, f: PP/ZnO-PDA membrane).

As the critical performance metric, conductivity also increases with the increase in resin content, driven by the enhanced ion mobility within the hydrated membrane. However, an outlier (R-55) deviates from the overall trend, likely due to minor inconsistencies in the fabrication process. Such variability underscores the importance of maintaining strict control over synthesis parameters to achieve reproducible performance.

Water permeability and vanadium permeability exhibit parallel trends, with higher resin content resulting in increased permeability values. This behavior is attributed to the expansion of the membrane hydrophilic regions, facilitating the transport of water and vanadium ions. While this enhances ionic transport, it also highlights a trade-off between conductivity and selectivity. Optimizing resin content is therefore crucial to achieving a balance suited for specific applications, such as VRFBs, where low vanadium crossover is essential.

### Effects of ZnO-PDA Loading

Figure 5 displays the influence of ZnO-PDA loading on membrane properties. The incorporation of ZnO nanoparticles significantly impacts water uptake, IEC, and conductivity. At low ZnO concentrations (up to 2.5 wt.%), water uptake increases due to the hydrophilic nature of ZnO (Ansari, 2024). This enhancement in hydration facilitates ion transport, resulting in higher IEC and conductivity. However, at higher ZnO concentrations (5–10 wt.%), water uptake declines.

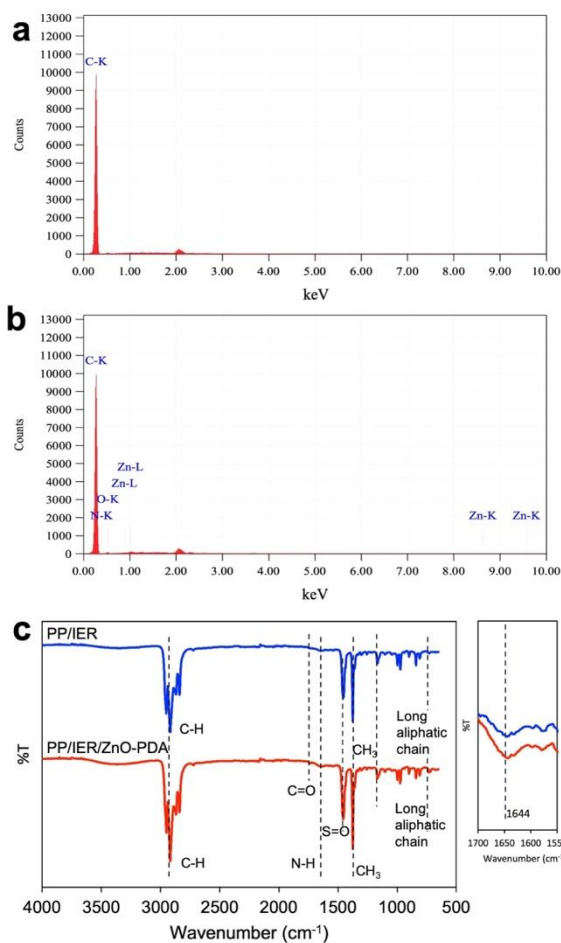


Figure 3. EDS spectra of (a) R-50 and (b) Z-10 membranes. (c) FTIR spectra of PP and PP/ZnO-PDA membranes (Z-10).

This reduction is attributed to the densification of the membrane matrix caused by ZnO aggregation, which restricts water permeation (Hosseini et al., 2012).

The relationship between ZnO loading and IEC mirrors this trend. Initially, ZnO nanoparticles provide additional active sites for ion adsorption, enhancing IEC. Beyond 2.5 wt.%, ZnO aggregation limits the accessibility of functional groups, leading to a decline in IEC. Conductivity follows a similar pattern, with an initial increase due to improved ion mobility and subsequent decreases at higher ZnO concentrations.

Water and vanadium permeability values decrease significantly with increasing ZnO content. This reduction is advantageous for VRFB applications, where minimizing vanadium crossover is critical. The reduction of permeability is likely due to the reduced void fraction within the membrane matrix, which restricts the ion transport channels. These findings align with previous studies that emphasize the role of ZnO in enhancing selectivity (Manzoor et al., 2024).

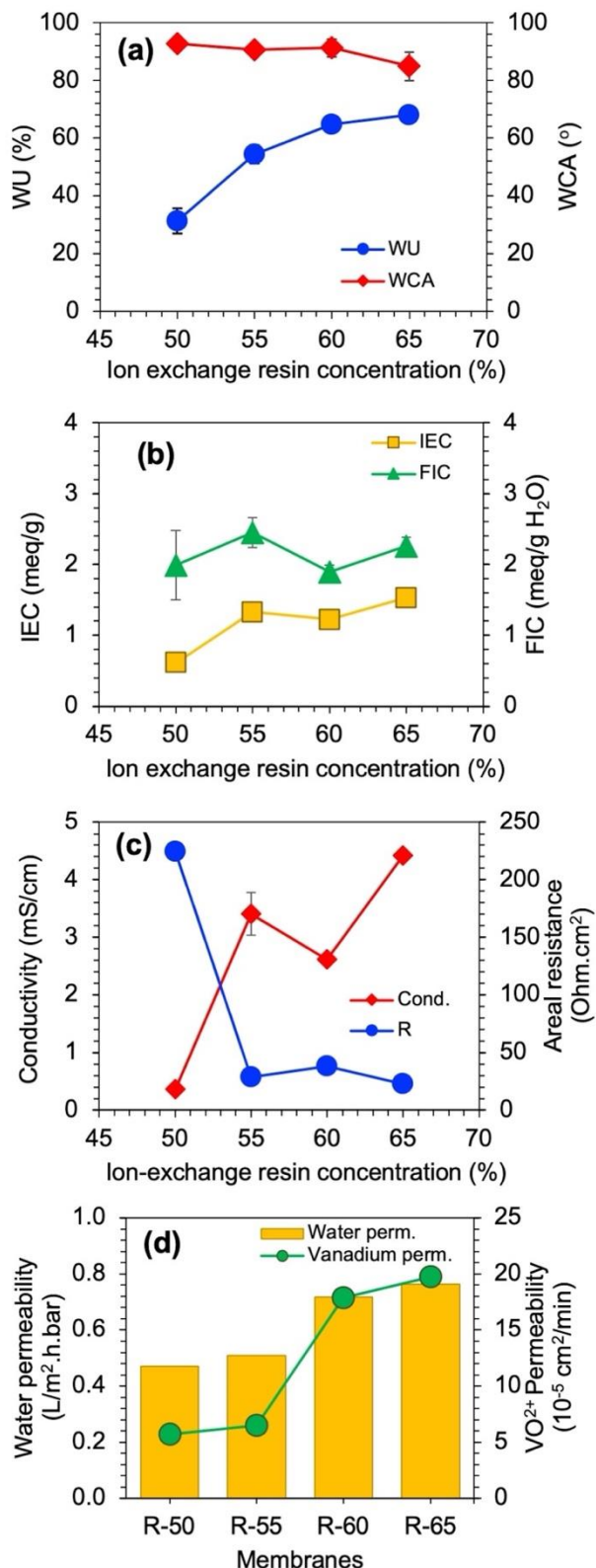


Figure 4. Effect of ion exchange resin content on membrane properties. (a) Water uptake (WU) and water contact angle (WCA). (b) Ion exchange capacity (IEC) and fixed ion concentration (FIC). (c) Conductivity and areal resistance. (d) Water and vanadium permeability.

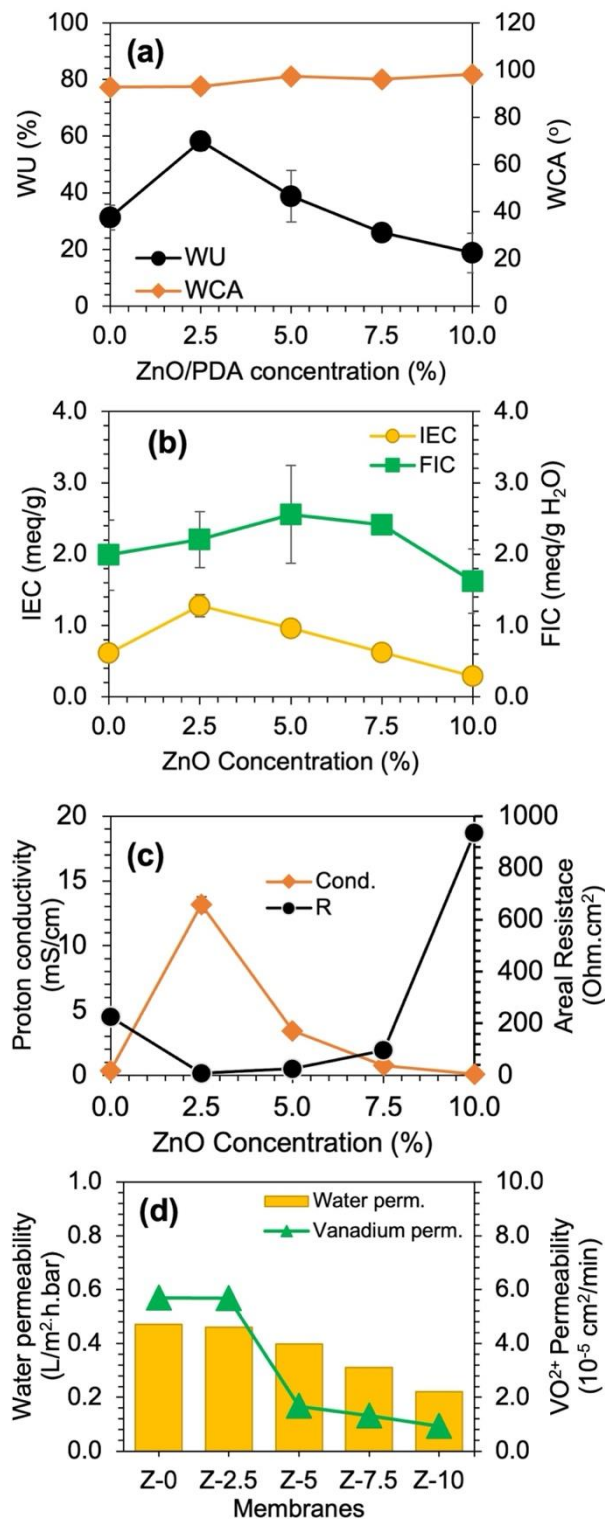


Figure 5. Effect of ZnO/PDA loading on membrane properties. (a) Water uptake (WU) and water contact angle (WCA). (b) Ion exchange capacity (IEC) and fixed ion concentration (FIC). (c) Conductivity and areal resistance. (d) Water and vanadium permeability.

Table 2 compares the performance of PP/ZnO-PDA membranes with other modified membranes. The Z-2.5 membrane demonstrates favorable selectivity characteristics, including reduced

water permeability ( $0.46 \text{ L}\cdot\text{m}^{-2}\cdot\text{h}^{-1}\cdot\text{bar}^{-1}$ ) and vanadium ion crossover ( $5.67 \times 10^{-5} \text{ cm}^2 \text{ min}^{-1}$ ). However, its proton conductivity ( $13.17 \text{ mS/cm}$ ) remains below that of high-performance alternatives, such as  $\text{TiO}_2/2$ -methylimidazole ( $63.69 \text{ mS/cm}$ ) and PTFE/Nafion ( $57.0 \text{ mS/cm}$ ).

The Z-10 membrane achieves even lower water permeability ( $0.22 \text{ L}\cdot\text{m}^{-2}\cdot\text{h}^{-1}\cdot\text{bar}^{-1}$ ), but at the expense of reduced conductivity ( $0.07 \text{ mS/cm}$ ) and higher vanadium permeability. These findings highlight the challenges of balancing conductivity and selectivity in the membrane design. Future research should be focused on mitigating ZnO aggregation and optimizing membrane hydration to enhance both performance metrics.

Figure 6 reveals strong positive correlations between IEC and conductivity, as well as between water uptake and vanadium permeability. Higher IEC enhances ion transport but increases vanadium crossover, illustrating a trade-off between conductivity and selectivity. WU improves hydration

and ionic mobility but compromises selectivity by increasing permeability. FIC positively influences conductivity, but its impact on permeability is minimal, emphasizing the need for structural modifications to control ion transport.

These results underscore the complexity of designing ion-exchange membranes for applications like VRFBs. Achieving the optimal balance between conductivity and selectivity requires advanced materials and structural modifications. Strategies, such as crosslinking, surface functionalization, and composite membrane fabrication can enhance performance while minimizing the possible trade-offs. Future research should be prioritized on the development of membranes with tailored hydration and structural features to meet the demanding requirements of energy storage systems.

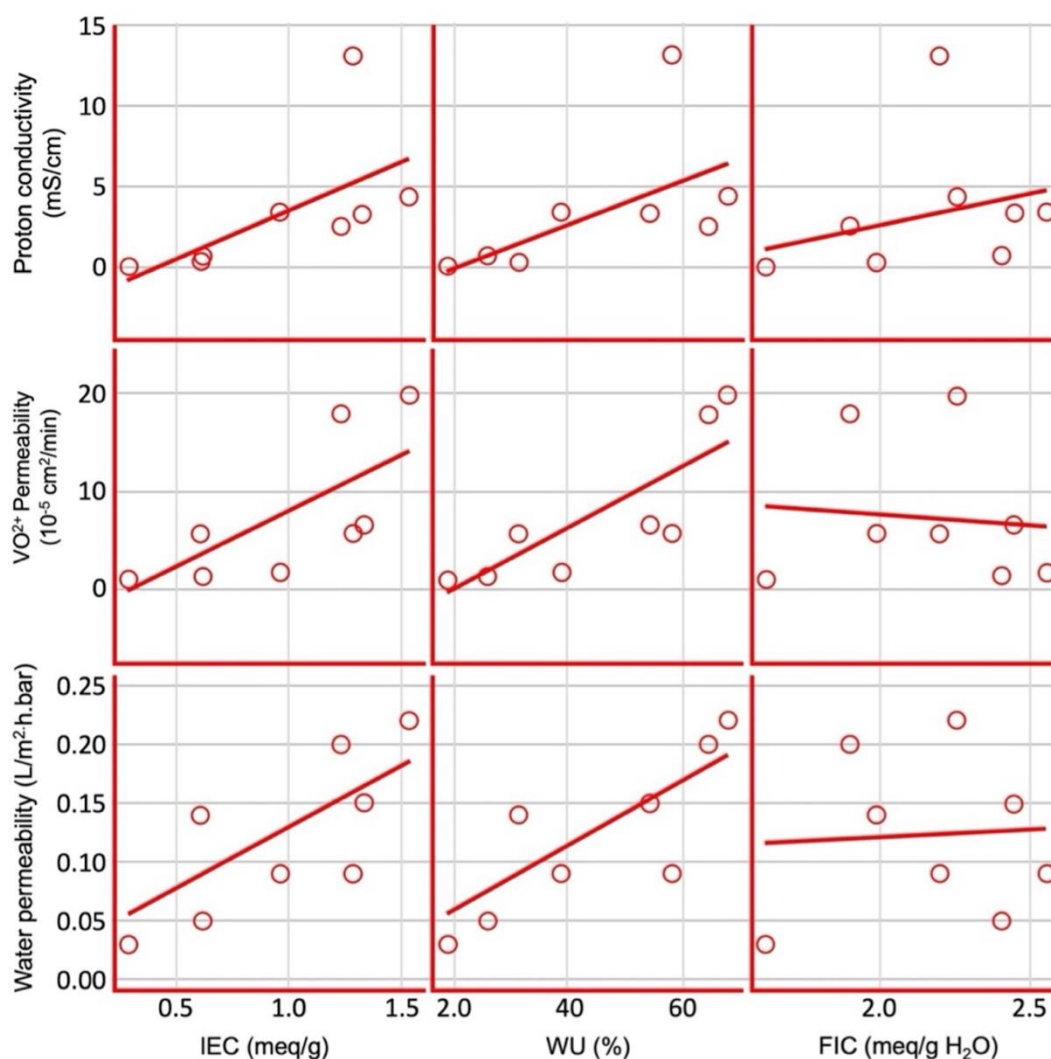


Figure 6. Effects of IEC, WU, and FIC.

Table 2. Comparative properties of membranes synthesized in this study and those reported in other studies

Membrane composition	Proton conductivity (mS/cm)	Water permeability ( $L \cdot m^{-2} \cdot h^{-1} \cdot bar^{-1}$ )	Vanadium permeability ( $cm^2 \cdot min^{-1}$ )	Refs.
TiO <sub>2</sub> and 2-methylimidazole	63.69	2.1	$1.73 \times 10^{-9}$	(Yan et al., 2016)
Polyimide	28.33	9.8	$7.53 \times 10^{-7}$	(Xu et al., 2022)
poly(benzimidazole)	16.6	16.5	$4.5 \times 10^{-8}$	(Luo et al., 2016)
Sulfonated polyether ether ketone/carbon active	19.12	10.09	$7.9 \times 10^{-8}$	(Lou et al., 2022)
Polyethylene	0.4	6.1	$1.19 \times 10^{-6}$	(Cao et al., 2016)
Polytetrafluoroethylene / Nafion	57.0	1.18	$1.2 \times 10^{-5}$	(Shi et al., 2019)
Nafion 117	5.75	4.7	$2.26 \times 10^{-5}$	(Wu et al., 2014)
Sulfonated poly(ether ether ketone)/Cationic covalent organic nanosheet (TpTG) crosslinked graphene oxide	82.7	-	$8.3 \times 10^{-7}$	(Zhang et al., 2025)
PP/ZnO-PDA (Z-2.5)	13.17	0.46	$5.67 \times 10^{-5}$	This work
PP/ZnO-PDA (Z-10)	0.07	0.22	$9.2 \times 10^{-6}$	This work

## CONCLUSION

This study successfully developed the heterogeneous cation-exchange membrane derived from PP and IER, modified with PDA-functionalized ZnO nanoparticles. The incorporation of ZnO-PDA into the membrane matrix effectively reduced both water permeability and vanadium ion crossover, with the PP/ZnO-PDA (Z-2.5) membrane achieving water permeability of  $0.46 L \cdot m^{-2} \cdot h^{-1} \cdot bar^{-1}$  and vanadium permeability of  $5.67 \times 10^{-5} cm^2 \cdot min^{-1}$ . However, the proton conductivity of the modified membranes, although moderate at 13.17 mS/cm, remains lower than that of high-performance membranes. The results further demonstrated that increasing the ZnO-PDA content beyond 2.5 wt.% led to decreases in WU, IEC, and proton conductivity, which is likely due to the aggregation of nanoparticle that reduced the access to ion-exchange sites. Although the addition of ZnO-PDA enhanced membrane selectivity, excessive loading diminished overall membrane performance. Additionally, an increase in IER concentration improved proton conductivity, IEC and increased vanadium permeability, revealing a trade-off between enhanced conductivity and selectivity. Further optimization is necessary to improve proton conductivity without compromising selectivity.

## ACKNOWLEDGEMENTS

This research is financially supported by “Penelitian, Pengabdian kepada Masyarakat, dan Inovasi (PPMI)”, ITB.

## REFERENCES

Alkhouzaam, A., Qiblawey, H., & Khraisheh, M. (2021). Polydopamine Functionalized Graphene Oxide as Membrane Nanofiller: Spectral and Structural Studies. In *Membranes* (Vol. 11, Issue 2). <https://doi.org/10.3390/membranes11020086>

Ansari, I. A. (2024). Advanced IPMC Actuators Utilizing Multifaceted Platinum-Coated Sulfonated Polyvinyl Alcohol-Graphene Oxide-Nanoform ZnO Nanocomposite Membranes. *Journal of Polymers and the Environment*, 32(9), 4466–4482. <https://doi.org/10.1007/s10924-024-03256-y>

Cao, L., Kronander, A., Tang, A., Wang, D. W., & Skyllas-Kazacos, M. (2016). Membrane permeability rates of vanadium ions and their effects on temperature variation in vanadium redox batteries. *Energies*, 9(12). <https://doi.org/10.3390/en9121058>

Choi, H. J., Youn, C., Kim, S. C., Jeong, D., Lim, S. N., Chang, D. R., Bae, J. W., & Park, J. (2022). Nafion/functionalized metal-organic framework composite membrane for vanadium redox flow battery. *Microporous and Mesoporous Materials*, 341, 112054. <https://doi.org/https://doi.org/10.1016/j.micromeso.2022.112054>

Cui, Y., Hu, Y., Wang, Y., Wang, Y., Peng, J., Li, J., & Zhai, M. (2022). Tertiary amino-modified GO/Nafion composite membrane with enhanced ion selectivity for vanadium redox flow batteries. *Radiation Physics and Chemistry*, 195, 110081. <https://doi.org/https://doi.org/10.1016/j.radphyschem.2022.110081>

Hosseini, S. M., Madaeni, S. S., Asiani, H., & Heidari, A. R. (2012). Preparation and Electrochemical Characterization of Monovalent Ion Selective Poly (Vinyl Chloride)-Blend-Poly (Styrene-Co-Butadiene) Heterogeneous Cation Exchange Membrane Coated with Poly (Methyl Methacrylate). *Separation Science and Technology (Philadelphia)*, 47(10), 1443–1454. <https://doi.org/10.1080/01496395.2011.645264>

- Jansen, J. C. (2016). Encyclopedia of Membranes. In E. Drioli & L. Giorno (Eds.), *Encyclopedia of Membranes*. Springer Berlin Heidelberg. <https://doi.org/10.1007/978-3-662-44324-8>
- Jiang, F., & Xue, R. (2023). Ion-Selective Membranes Fabricated Using Finely Controlled Swelling of Non-Ionic Fluoropolymer for Redox Flow Batteries. *Batteries*, 9(11), 545. <https://doi.org/10.3390/batteries9110545>
- Khoiruddin, K., Ariono, D., Subagjo, S., & Wenten, IG. (2020). Structure and transport properties of polyvinyl chloride-based heterogeneous cation-exchange membrane modified by additive blending and sulfonation. *Journal of Electroanalytical Chemistry*, 873, 114304. <https://doi.org/10.1016/j.jelechem.2020.114304>
- Kugarajah, V., Sugumar, M., Swaminathan, E., Balasubramani, N., & Dharmalingam, S. (2021). Investigation on sulphonated zinc oxide nanorod incorporated sulphonated poly (1,4-phenylene ether ether sulfone) nanocomposite membranes for improved performance of microbial fuel cell. *International Journal of Hydrogen Energy*, 46(42), 22134–22148. <https://doi.org/https://doi.org/10.1016/j.ijhydene.2021.04.067>
- Li, J., Xu, F., Chen, W., Han, Y., & Lin, B. (2023). Anion Exchange Membranes Based on Bis-Imidazolium and Imidazolium-Functionalized Poly(phenylene oxide) for Vanadium Redox Flow Battery Applications. *ACS Omega*, 8(18), 16506–16512. <https://doi.org/10.1021/acsomega.3c01846>
- Li, L., Wei, G., Liu, H., Guo, Y., & Ma, Y. (2024). Constructing amino-functionalized flower-shaped ZnO@Al<sub>2</sub>O<sub>3</sub> nanofibers composite membrane (ZANFs/SPSF) with hierarchical proton conductive pathways and excellent methanol resistance. *Journal of Membrane Science*, 697, 122525. <https://doi.org/10.1016/j.memsci.2024.122525>
- Liang, D., Wang, S., Ma, W., Wang, D., Liu, G., Liu, F., Cui, Y., Wang, X., Yong, Z., & Wang, Z. (2022). A low vanadium permeability sulfonated polybenzimidazole membrane with a metal-organic framework for vanadium redox flow batteries. *Electrochimica Acta*, 405, 139795. <https://doi.org/https://doi.org/10.1016/j.electacta.2021.139795>
- Liu, D., Ma, L., Liu, L., Wang, L., Liu, Y., Jia, Q., Guo, Q., Zhang, G., & Zhou, J. (2016). Polydopamine-Encapsulated Fe<sub>3</sub>O<sub>4</sub> with an Adsorbed HSP70 Inhibitor for Improved Photothermal Inactivation of Bacteria. *ACS Applied Materials and Interfaces*, 8(37), 24455–24462. <https://doi.org/10.1021/acsomega.6b08119>
- Long, J., Yang, H., Wang, Y., Xu, W., Liu, J., Luo, H., Li, J., Zhang, Y., & Zhang, H. (2020). Branched Sulfonated Polyimide/Sulfonated Methylcellulose Composite Membranes with Remarkable Proton Conductivity and Selectivity for Vanadium Redox Flow Batteries. *ChemElectroChem*, 7(4), 937–945. <https://doi.org/10.1002/celec.201901887>
- Lou, X., Lu, B., He, M., Yu, Y., Zhu, X., Peng, F., Qin, C., Ding, M., & Jia, C. (2022). Functionalized carbon black modified sulfonated polyether ether ketone membrane for highly stable vanadium redox flow battery. *Journal of Membrane Science*, 643(September 2021), 1–8. <https://doi.org/10.1016/j.memsci.2021.120015>
- Luo, T., David, O., Gendel, Y., & Wessling, M. (2016). Porous poly(benzimidazole) membrane for all vanadium redox flow battery. *Journal of Power Sources*, 312, 45–54. <https://doi.org/10.1016/j.jpowsour.2016.02.042>
- Manzoor, Q., Farrukh, M. A., & Sajid, A. (2024). Optimization of lead (II) and chromium (VI) adsorption using graphene oxide/ZnO/chitosan nanocomposite by response surface methodology. *Applied Surface Science*, 655, 159544. <https://doi.org/10.1016/j.apsusc.2024.159544>
- Mezher, H. M., Adeli, H., & Alsally, Q. F. (2024). Novel ZnO-Modified Polyethersulfone Nanocomposite Membranes for Nanofiltration of Concentrated Textile Wastewater. *Water, Air, & Soil Pollution*, 235(2), 138. <https://doi.org/10.1007/s11270-024-06927-7>
- Mohammed, A., & Abdullah, A. (2018). Scanning Electron Microscopy (Sem): a Review. *Proceedings of 2018 International Conference on Hydraulics and Pneumatics - HERVEX*, 77–85.
- Oreiro, S. N., Sloth, J., Bentien, A., Madsen, M. B., & Drechsler, T. (2025). Crossover mitigation strategies in a commercial 6 kW/43kAh vanadium redox flow battery. *Journal of Energy Storage*, 107, 115032. <https://doi.org/10.1016/j.est.2024.115032>
- Palanisamy, G., & Oh, T. H. (2022). TiO<sub>2</sub> Containing Hybrid Composite Polymer Membranes for Vanadium Redox Flow Batteries. In *Polymers* (Vol. 14, Issue 8). <https://doi.org/10.3390/polym14081617>
- Shi, W., Liu, X., Ye, C., Cao, X., Gao, C., & Shen, J. (2019). Efficient lithium extraction by membrane capacitive deionization incorporated with monovalent selective cation exchange membrane. *Separation and Purification Technology*, 210, 885–890. <https://doi.org/10.1016/j.seppur.2018.09.006>

- Vyas, P. V., Ray, P., Adhikary, S. K., Shah, B. G., & Rangarajan, R. (2003). Studies of the effect of variation of blend ratio on permselectivity and heterogeneity of ion-exchange membranes. *Journal of Colloid and Interface Science*, 257(1), 127–134. [https://doi.org/http://dx.doi.org/10.1016/S0021-9797\(02\)00025-5](https://doi.org/http://dx.doi.org/10.1016/S0021-9797(02)00025-5)
- Wang, Y., Mu, A., Wang, W., Yang, B., & Wang, J. (2024). A Review of Capacity Decay Studies of All-vanadium Redox Flow Batteries: Mechanism and State Estimation. *ChemSusChem*, 17(14). <https://doi.org/10.1002/cssc.202301787>
- Wardani, A. K., Ariono, D., Subagjo, S., & Wenten, I. G. (2020a). Fouling tendency of PDA/PVP surface modified PP membrane. *Surfaces and Interfaces*, 19, 100464. <https://doi.org/10.1016/j.surfin.2020.100464>
- Wardani, A. K., Ariono, D., Subagjo, S., & Wenten, I. G. (2020b). Fouling tendency of PDA/PVP surface modified PP membrane. *Surfaces and Interfaces*, 19, 100464. <https://doi.org/10.1016/j.surfin.2020.100464>
- Wardani, A. K., Ariono, D., Subagjo, & Wenten, I. G. (2019a). Hydrophilic modification of polypropylene ultrafiltration membrane by air-assisted polydopamine coating. *Polymers for Advanced Technologies*, 30(4), 1148–1155. <https://doi.org/10.1002/pat.4549>
- Wardani, A. K., Ariono, D., Subagjo, & Wenten, I. G. (2019b). Hydrophilic modification of polypropylene ultrafiltration membrane by air-assisted polydopamine coating. *Polymers for Advanced Technologies*, 30(4), 1148–1155. <https://doi.org/10.1002/pat.4549>
- Wenten, I. G., Khoiruddin, K., & Siagian, U. W. R. (2024). Green Energy Technologies: A Key Driver in Carbon Emission Reduction. *Journal of Engineering and Technological Sciences*, 56(2), 143–192. <https://doi.org/10.5614/j.eng.technol.sci.2024.56.2.1>
- Wu, X., Hu, J., Liu, J., Zhou, Q., Zhou, W., & Li, H. (2014). Ion exchange membranes for vanadium redox flow batteries. *Pure and Applied Chemistry*, 86(5), 633–649. <https://doi.org/10.1515/pac-2014-0101>
- Xu, W., Long, J., Liu, J., Luo, H., Duan, H., Zhang, Y., Li, J., Qi, X., & Chu, L. (2022). A novel porous polyimide membrane with ultrahigh chemical stability for application in vanadium redox flow battery. *Chemical Engineering Journal*, 428(July 2021), 131203. <https://doi.org/10.1016/j.cej.2021.131203>
- Yan, H.-F., Luo, L.-H., Xu, Z.-L., Fang, Y.-X., Pandaya, D., Dai, J.-Y., Liang, J., & Xu, S.-J. (2024). Incorporating etched ZnO nanoparticles to fabricate positively charged composite membrane for heavy metal removal. *Desalination*, 574, 117275. <https://doi.org/10.1016/j.desal.2023.117275>
- Yan, L., Li, D., Li, S., Xu, Z., Dong, J., Jing, W., & Xing, W. (2016). Balancing Osmotic Pressure of Electrolytes for Nanoporous Membrane Vanadium Redox Flow Battery with a Draw Solute. *ACS Applied Materials and Interfaces*, 8(51), 35289–35297. <https://doi.org/10.1021/acsami.6b12068>
- Yang, J., Peng, Z., Tang, W., Lv, P., & Wang, Q. (2024). Enhanced Vanadium Redox Flow Battery Performance with New Amphoteric Ion Exchange Membranes. *Macromolecular Rapid Communications*, 45(22). <https://doi.org/10.1002/marc.202400477>
- Yang, L., Liu, X., Zhang, X., Chen, T., Ye, Z., & Rahaman, Md. S. (2022). High performance nanocomposite nanofiltration membranes with polydopamine-modified cellulose nanocrystals for efficient dye/salt separation. *Desalination*, 521, 115385. <https://doi.org/https://doi.org/10.1016/j.desal.2021.115385>
- Ye, J., Yuan, D., Ding, M., Long, Y., Long, T., Sun, L., & Jia, C. (2021). A cost-effective nafion/lignin composite membrane with low vanadium ion permeation for high performance vanadium redox flow battery. *Journal of Power Sources*, 482(October 2020), 229023. <https://doi.org/10.1016/j.jpowsour.2020.229023>
- Zhai, S., Lu, Z., Ai, Y., Liu, X., Wang, Q., Lin, J., He, S., Tian, M., & Chen, L. (2022). Highly selective proton exchange membranes for vanadium redox flow batteries enabled by the incorporation of water-insoluble phosphotungstic acid-metal organic framework nanohybrids. *Journal of Membrane Science*, 645, 120214. <https://doi.org/https://doi.org/10.1016/j.memsci.2021.120214>
- Zhang, Y., Liu, H., Liu, M., Li, X., Zhang, Y., Sun, H., Shi, H., & Feng, Y. (2025). Enhanced selectivity of SPEEK membrane incorporated covalent organic nanosheet crosslinked graphene oxide for vanadium redox flow battery. *Journal of Membrane Science*, 714, 123410. <https://doi.org/10.1016/j.memsci.2024.123410>